Nanoscale

Accepted Manuscript

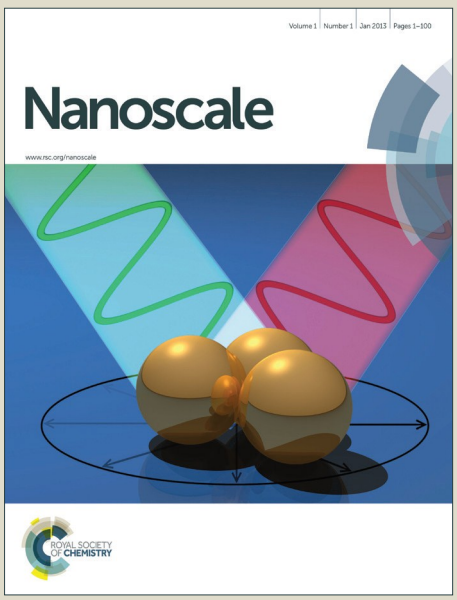

ROYAL SOCIETY OF CHEMISTRY

www.rsc.org/nanoscale

Journal Name

ARTICLE

Highly Selective Luminescent Nanostructures for Mitochondria Imaging and Targeting

Received 00th January 20xx,
Accepted 00th January 20xx

DOI: 10.1039/x0xx00000x

www.rsc.org/

E. Fanizza,[a,b,†] R. M. Iacobazzi,[c,d,†] V. Laquintana,[c] G. Valente,[a,b] G. Caliandro,[a] M. Striccoli,[b] A. Agostiano,[a,b] A. Cutrignelli,[c] A. Lopedota,[c] M. L. Curri,[b] M. Franco,[c] N. Depalo,[b,*] N. Denora[c,*]

Here a luminescent hybrid nanostructure based on functionalized quantum dots (QDs) is used as fluorescent imaging agent able to target selectively mitochondria thanks to the molecular recognition of the translocator protein (TSPO). The selective targeting of such 18-kDa protein mainly located in the outer mitochondrial membrane and overexpressed in several pathological states including neurodegenerative diseases and cancers, may provide valuable information for the early diagnosis and therapy of human disorders. In particular, the rational design of amino functionalized luminescent silica coated QD nanoparticles (QD@SiO_2 NPs) provides a versatile nanoplatform to anchor a potent and selective TSPO ligand, characterized by a 2-phenyl-imidazo[1,2-a]pyridine acetamide structure along with a derivatizable carboxylic end group, useful to conjugate the TSPO ligand and achieve TSPO-QD@SiO_2 NPs by means of a covalent amide bond. Colloidal stability and optical properties of the proposed nanomaterials are comprehensively investigated and their potential as mitochondrial imaging agents fully assessed. Sub-cellular fractionation, together with confocal laser scanning fluorescence microscopy and co-localization analysis of targeted TSPO-QD@SiO_2 NPs in C6 glioma cells overexpressing the TSPO, prove the great potential of these multifunctional nanosystems as *in vitro* selective mitochondrial imaging agent.

Introduction.

Colloidal nanoparticle (NP) based formulations are emerging as revolutionary clinical tools to design efficient subcellular-targeted contrast agents and/or drug delivery nanosystems.[1,2] Targeting and delivery at subcellular level have become increasingly important to understand complex events that occur within living cells and, thus, to design suitable therapies for the treatment of specific diseases.[3] Among the cellular organelles, mitochondria represent an important subcellular target, not only for their extremely relevant functions, but also because their dysfunctions or damage may contribute to various human disorders, such as cancer, neurodegenerative and neuromuscular diseases, cardiac problem, aging, diabetes, and obesity.[4] While several examples of NP based diagnostic and/or therapeutic systems for the imaging and/or treatment, respectively, of non-mitochondrial diseases have been reported so far,[1,5] only limited progress has been achieved in the development of multifunctional colloidal NPs for the diagnosis and cure of mitochondrial dysfunction-associated disorders.[2,6]

Currently available mitochondria imaging probes are mainly organic dyes, such as JC1, MitoTracker, having a chemical structure suitably designed to bind to the negatively charged outer mitochondrial membrane (OMM) and resulting in a fluorescent signal.[7,8] Unfortunately, such organic fluorophores have been reported to be susceptible to photobleaching under continuous light exposure and to have short fluorescence (PL) lifetimes, thus preventing time-gated detection.[7,8] These limitations make them less attractive labels for durable and sensitive imaging and, therefore, new photostable molecular probes are under development.[9] In this regard, a great advantage arises from the exploitation of semiconductor luminescent nanocrystals, namely quantum dots (QDs), as fluorescent contrast agents characterized by superior photostability.[10] Compared to organic dyes, QDs have a broad absorption spectrum, a narrow and mainly symmetric emission band, long PL lifetimes, which permits long-term and sensitive bio-imaging, even at the single molecule level.[9] So far, only very few examples of QD-based nanostructures have been proposed as fluorescent nanoprobes for selective mitochondrial targeting. These reports concern QDs functionalized with peptides or small molecules for specific labeling of mitochondria. An oligopeptide derived from the cytochrome-C oxidase enzyme has been demonstrated to penetrate across the cellular membrane and transport QDs specifically to the mitochondria in living cells.[11] Very recently,

[a] *Dipartimento di Chimica, Università degli Studi di Bari "Aldo Moro", Via Orabona 4, 70126 Bari, Italy*
[b] *CNR Istituto per i Processi Chimico Fisici IPCF Consiglio Nazionale delle Ricerche CNR, via Orabona 4, 70126 Bari, Italy*
[c] *Dipartimento di Farmacia – Scienze del Farmaco, Università degli Studi di Bari "Aldo Moro", Via Orabona 4, 70126 Bari, Italy.*
[d] Istituto Tumori IRCCS Giovanni Paolo II, Bari, Italy
†These authors contributed equally.
Electronic Supplementary Information (ESI) available: Additional TEM micrographs, fluorescent and UV-Vis absorbance spectra of silica coated QD nanoparticles and TSPO ligand are reported in the Electronic Supplementary Information. See DOI: 10.1039/x0xx00000x

triphenylphopshonium (TPP), a lipophilic cation molecule, widely used for mitochondria targeting, has been covalently conjugated to the surface of polyacrylate coated QDs, decorated with sulphonate and amine functional groups which induce endosomal escape.[12] Similarly, poly(lactic-co-glycolic acid) based luminescent QDs have been functionalized with TPP molecules and used for delivery of mitochondria-acting therapeutics.[2] In the latter examples, the preferential uptake of these cationic functionalized QDs within mitochondria has been driven by the very negative membrane potential across the inner mitochondrial membrane.

In this work, mitochondrial targeting has been investigated with an original and innovative strategy based on the identification of an interesting OMM biomarker. In particular, positively charged luminescent core-shell (CdSe)ZnS QD-based nanostructures, surface functionalized with amino groups, have been conjugated with a synthetic ligand, suitably designed for the selective recognition of the mitochondrial translocator protein 18-kDa (TSPO). TSPO, first known as the peripheral-type benzodiazepine receptor, is a five-transmembrane domain protein which is mainly located in the OMM, whose biological role is associated to mitochondrial function, steroidogenesis and cell proliferation/apoptosis.[13-17] Interestingly, aberrant TSPO levels have been observed in multiple diseases, including cancer and neurodegenerative disorders. Thus, TSPO is considered an extremely attractive subcellular target, useful to chart its distribution in disease states, overexpressing this protein as well as to achieve a selective mitochondrial drug targeting.[18-21] Several high binding affinity and selective small molecules have been developed as TSPO ligands and many of them are currently explored in positron emission tomography (PET),[22] magnetic resonance (MR) and optical imaging.[13, 23] Among these techniques, fluorescence imaging emerges as rich in contrast and versatile diagnostic tool with high sensitivity and selectivity.[24,25] Consequently, the research and development of new fluorescent TSPO ligands has been actively pursued, and several promising candidates have been proposed to potentially replace the currently most used TSPO radioligands.[25] Even though numerous TSPO-selective labels have been investigated to date, the concept of mitochondrial imaging through TSPO targeted NPs has been poorly explored due to several reasons, including the identification of potent and selective TSPO ligands containing organic functions enabling their further conjugation on the NP surface without endangering their capacity to recognize the mitochondrial protein. In this perspective, among the very few examples of TSPO-targeted NPs imaging agents, we have recently reported luminescent organic poly(amidoamine) dendrimers of fourth generation [G(4)-PAMAM], properly targeted to the mitochondria by TSPO molecular recognition.[26, 27] In particular, the multiple surface amino end groups, available on the dendrimer, have been exploited for the attachment of both an organic fluorescent tag, namely fluorescein isothiocyanate (FITC), and a specific molecular domain that selectively recognizes TSPO, characterized by a 2-phenyl-imidazo[1,2-a]pyridine acetamide structure and an easily conjugable carboxylic moiety. The selective mitochondrial targeting achieved by the TSPO targeted-G(4)-PAMAM–FITC dendrimers has established the molecular recognition ability of the synthetic TSPO ligand.[27] However, such "*soft*" luminescent TSPO targeted nanocarrier, although selective for mitochondria, still suffers from the main limitations arising from the use of the organic fluorophore FITC.

Therefore, specific efforts have been devoted in the development of TSPO-targeted NPs for mitochondria labeling to achieve the challenging rational design of a novel, robust nanostructure. In such nanosystems, G(4)-PAMAM–FITC dendrimers have been replaced by QDs as PL probes, taking, thus, advantage of their superior photophysical properties[10] and versatile surface chemistry.[28] In particular here, amine functionalized luminescent silica coated (CdSe)ZnS QDs (NH_2-QD@SiO_2 NPs) have been successfully conjugated to the synthetic TSPO ligand, previously reported by Denora et al.,[27] thus resulting in a single object nanoarchitecture, where the selectivity of the ligand towards TSPO and the photostability and high luminescence of the inorganic QDs have been effectively and successfully conveyed. In this study hydrophobic luminescent QDs have been suitably engineered, by controlling size, shape and surface charge, in order to ensure water dispersibility, to induce cell internalization and delivery to the mitochondria, preserving the colloidal stability and optical properties. Encapsulation of QDs in silica shells can significantly improve their stability in the aqueous phase,[29-31] as silica is an inert, biocompatible and transparent material, able to reduce the release of cytotoxic ions and to prevent QD photo-oxidation.[32] Silica coated QD represents a robust inorganic system, characterized by a high chemical stability, an intrinsic hydrophilicity and highly versatile surface, suited to be functionalized by TSPO targeting ligand molecules. The proposed nanostructure offers, in principle, a great advantage compared to the previously reported systems. Indeed it ingeniously combines photophysical stability of QDs, versatility of the surrounding silica shell, which represents an amenable scaffold for the further conjugation with biorecognition entities and/or therapeutic agents, and the targeted properties of the synthetic ligand, selectively recognizing TSPO, and hence able to deliver the NPs to the mitochondria.[28] The physical and chemical characteristics of this functional nanomaterial have been comprehensively investigated by means of morphological, structural and optical investigations, while *in vitro* studies by subcellular fractionation and confocal laser scanning fluorescence microscopy and co-localization analysis have finally proven the success of the nanostructures in targeting mitochondria by means of TSPO molecular recognition.

Results and discussion

In this work, luminescent QDs have been proposed as inorganic fluorophore elements for the selective targeting and bioimaging of mitochondria. Scheme 1 (panel A and C) reports the route to achieve the fabrication of the targeted nanostructure. The general concept is to label QD@SiO_2 NPs

with a synthetic moiety characterized by a 2-phenyl-imidazo[1,2-a]pyridine acetamide structure, able to accomplish recognition of TSPO receptor (Scheme 1 B and 1 C). The design of the nanostructure has to tackle some relevant issues for successfully accomplishing TSPO ligand-conjugated QD@SiO_2 NPs (TSPO-QD@SiO_2 NPs) to be applied as mitochondria luminescent probes. Indeed, nanostructure size, surface charge and chemistry need to be carefully tailored to enhance the (intra)cellular uptake, but also to induce endosomal escape, which is strictly required for an effective subcellular targeting. Furthermore, the process of cellular internalization should not radically alter the photophysical properties of the QDs, in order to limit quenching phenomena and thus allow TSPO-QD@SiO_2 NPs for mitocondrial localization, by means of optical detection of the fluorescent signal.

Finally, the selectivity to mitochondria requires an effective binding of the TSPO biorecognition element, which should preserve its biological function upon the conjugation to NPs.

In this perspective, recently some of the authors have designed and synthesized a new TSPO drug ligand characterized by a 2-phenylimidazo[1,2-a]pyridine acetamide structure containing a derivatizable carboxylic handle.[27, 33]

The chemical modification has led to the identification of a potent and selective TSPO ligand with a carboxylic conjugable function, which has been successfully anchored to fluorescent G(4)-PAMAM dendrimers retaining its binding affinity toward the mitochondrial translocator protein 18-kDa. Starting from such an evidence an original nanostructure, based on the TSPO conjugated to QD@SiO_2 NP, has been here developed,

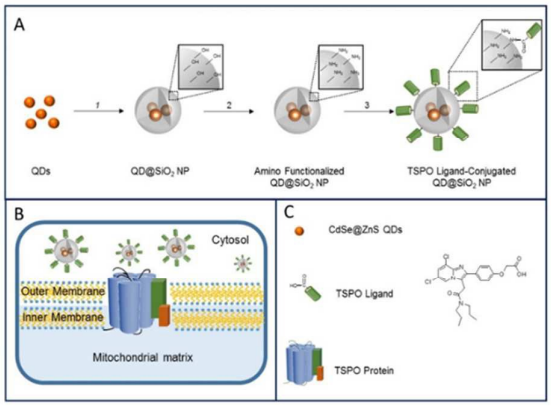

characterized and investigated as powerful tool to image *in vitro* the mitochondria, using a proper combination of complementary characterization techniques.

Scheme 1. Panel A, fabrication route of TSPO ligand-conjugated QD@SiO_2 NPs by coating QDs (step 1) with a silica shell, which is functionalized with amine groups, through reaction with 3-(aminopropyl) trimethoxysilane, (step 2), and further conjugated to TSPO (step 3). Panel B, Schematic illustrations of molecular recognition process between TSPO ligand-conjugated QD@SiO_2 NPs and TSPO protein, mainly located in the outer mitochondrial membrane. Panel C, legend containing a list of the single sketches depicted in the charts A and B.

Morphological and optical characterization of TSPO-QD@SiO_2 NPs.

The exceptional photophysical properties of hydrophobic QDs have been here exploited for the development of a fluorescent probe highly selective for mitochondria targeting. A silica shell coating the QDs has been grown by water-in-oil microemulsion approach[30,31,34] (Scheme 1A step 1, Electronic Supplementary Information Figure S 1) to attain NPs dispersible in a aqueous medium, to protect QDs, avoiding quenching phenomena, and limit the release of cytotoxic heavy metal ions from the QDs to the surrounding environment. This strategy allows to control the synthesis of core-shell QD@SiO_2 NPs in a size regime of few tens of nanometer in diameter, that is considered in principle the ideal NP size to efficiently penetrate the cell membrane.[35] Moreover, as previously reported,[30,31,34] core-shell nanostructure size distribution, core multiplicity and silica shell thickness, which are crucial factors for the application of these nanostructures as optical probes in vitro, can be effectively controlled by playing with water-in-oil microemulsion composition, and QD and silica shell precursor (TEOS) concentration. While the size and size distribution regulate the cellular uptake, the silica shell thickness and uniformity has impact on the nanostructure photostability in vitro. Therefore, here, suitable QDs and TEOS molar ratio have been selected in order to achieve colloidal QD@SiO_2 nanostructures quite small in size (26 nm), with a good monodispersity ($\sigma_{\%}$ = 15%) and with a silica shell 10 nm ($\sigma_{\%}$=17%) thick (See Electronic Supplementary Information Figure S 1B), that homogeneously coats the QDs. Such a shell thickness is large enough to isolate QDs form the environment, limiting quenching phenomena, and hence resulting in a robust optical probe for imaging in vitro (See Electronic Supplementary Information Figure S2). In fact

A not homogeneous and too thin (< 10 nm) silica shell cannot efficiently prevent interaction of the QDs with the physiological medium, thus inducing emission quenching. NH_2 groups have been grafted on the surface of the emitting NPs by reaction with 3-(aminopropyl) trimethoxysilane, (NH_2-QD@SiO_2 NPs Scheme 1, step 2) in order to provide anchoring sites for the subsequent binding with TSPO, by exploiting the reactive carboxylic group, purposely designed and introduced in the molecular structure of the TSPO ligand, to make possible further conjugation reaction. Among the different reported protocols, here, the conjugation reaction has been performed dispersing both NH_2-QD@SiO_2 NPs and the TSPO ligand in ethanol, and using BOP as coupling agent and DIPEA as organic amine, which regulates pH, promotes activation of the carboxylic moieties of the ligands and induces the fast aminolysis reaction.[33] The molar ratio of NH_2 groups, calculated according to the well-established ninhydrin test (See Experimental Section paragraph 4.2), and TSPO ligand has been fixed at nearly 5. In particular NH_2-QD@SiO_2 NPs containing 2.2 µmol of NH_2 groups reacted with 0.4 µmol of TSPO ligand in presence of crosslinking agents, as reported in the experimental section. It is worth to note that this reaction condition, characterized by use of a large excess of NH_2 groups

compared to the amount of the TSPO ligand, has been purposely selected in order to achieve only a partial neutralization of NH_2 groups upon conjugation. In fact, the high binding ability, demonstrated in previous works by the TSPO ligand, suggested that the targeting moiety exposed on the surface of TSPO-QD@SiO_2 NPs could effectively recognize mitochondria, even at low concentration.[27] While, instead, the presence of residual free NH_2 groups at the surface of TSPO-QD@SiO_2 NPs could enhance their colloidal stability in the physiological medium and provide a positively charged surface, which favors TSPO targeted NP internalization and subsequent delivery to mitochondria. Finally, additional free NH_2 groups could remain available for possible further conjugation with therapeutics and/or other biorecognition entities.

In Figure 1 and Figure 2 the optical and morphological analysis of the TSPO-QD@SiO_2 NPs are reported. The UV-Vis absorption spectrum (Figure 1B) combines the characteristic absorption features of the TSPO ligand (the two bands centered, respectively, at 254 and 333 nm, Figure 1A green line), with the UV-Vis absorption line shape of the NH_2-QD@SiO_2 NPs (Figure 1A blue line), thus highlighting the success of the conjugation reaction under the specific experimental conditions, namely, type of conjugation reaction, reagent molar ratio, reaction medium, temperature and time.

The UV-Vis absorbance spectrum of the TSPO-QD@SiO_2 suspension (Figure 1B) allows to estimate the concentration of bound TSPO ligand in the whole sample, as described in the experimental section. Starting from 0.3 mg/mL of NH_2-QD@SiO_2 NP suspension containing 2.2 µmol/mL of NH_2 groups, the concentration of TSPO ligand has been found of about 24 µg/mL (0.05 µmol of TSPO in 1 mL TSPO-QD@SiO_2 NP suspension, few hundreds of TSPO molecules per NP), thus a large amount of free NH_2 groups are expected to be found.

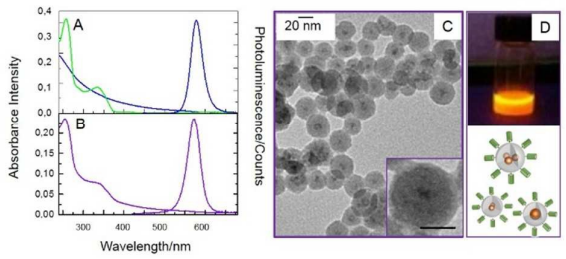

Figure 1. UV-Vis absorbance and PL spectra of diluted suspensions (1:20) of amino functionalized-QD@SiO_2 NPs (Panel A blue line) and TSPO ligand-conjugated QD@SiO_2 NPs (Panel B purple line) along with the UV-Vis absorbance spectra of TSPO ligand solution 10 µM (Panel A, green line) in ethanol. TEM micrograph of TSPO ligand-conjugated QD@SiO_2 NPs (Panel C, scale bar inset 10 nm), sketch of the nanostructure and picture of the sample upon UV lamp illumination (Panel D).

Remarkably the sample preserves the pristine emission properties of the QDs, showing a narrow PL band centred at 575 nm [λ_{ex}= 400 nm, slightly red shifted compared to the QD cores (See Electronic Supplementary Information Figure S 2)],[34] corresponding to the orange region of the visible spectrum, as also revealed from the UV lamp illuminated sample (Figure 1D).In addition, a minor PL blue shift can be observed moving from the NH_2-QD@SiO_2 NP (Figure 1A blue line) to the TSPO-QD@SiO_2 NP (Figure 1B, violet line) spectrum, reasonably ascribed to the further processing of sample for the TSPO bioconjugation, that may have removed a fraction of nanoparticles, likely those at higher core multiplicity.[34] The relative quantum yield of TSPO-QD@SiO_2 NPs ($QY_{TSPO\text{-}QD@SiO2}$ = 11%), results only slightly decreased compared to NH_2-QD@SiO_2 NPs ($QY_{NH2\text{-}QD@SiO2}$ = 15%), confirming the retention of the peculiar optical properties of luminescent QDs.

In order to rule out any contribution due to non-specific absorption of the TSPO ligand on surface of NH_2-QD@SiO_2 NPs, a mixture containing NH_2-QD@SiO_2 NPs and free TSPO ligand, has been incubated without any linker, under the same optimized experimental conditions for the preparation of the TSPO-QD@SiO_2 NPs. After purification, UV-Vis absorption measurements have been performed on the recovered NPs (See Electronic Supplementary Information Figure S 3B). Any characteristic absorption features of the TSPO ligand have been detected in the UV-Vis absorption spectrum of the purified mixture, thus indicating that the formation of a covalent bond takes place only when the conjugation reaction takes place in presence of cross linking agents, as previously described.

FTIR analysis of QD@SiO_2 NPs before and after conjugation with the TSPO ligand is reported in Figure 2, along with the FTIR spectra of the TSPO ligand alone (Figure 2A-B). The FTIR spectrum of the TSPO-QD@SiO_2 NPs (Figure 2C-D) clearly

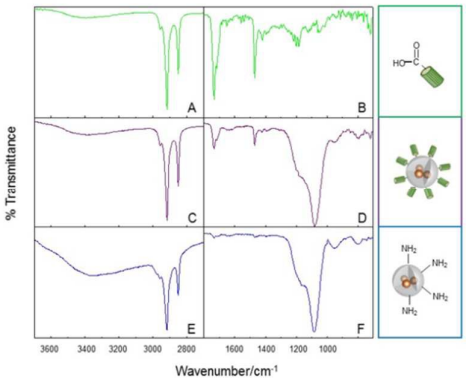

shows two peaks at 1739 and 1475 cm^{-1} that can be ascribed to the stretching of the amide group and the symmetric stretching of the C=C of the aromatic ring of the TSPO ligand, respectively. Furthermore, an intense band from 1200-1000 cm^{-1}, attributed to the symmetric and asymmetric stretching modes of the siloxane network Si-O-Si of the silica shell, is visible.

Figure 2. FTIR spectra of TSPO ligand (A, B), TSPO ligand-conjugated QD@SiO_2 NPs (C, D) and amino functionalized-QD@SiO_2 NPs (E, F) along with the sketches of TSPO ligand molecule and nanostructures.

In addition, a structural investigation of the TSPO-QD@SiO_2 NPs has been carried out by means of TEM investigation, DLS analysis and ζ-potential measurements, since the application

of a such hybrid nanostructures as imaging probe at subcellular level needs the accurate control of size, morphology and surface charge. Indeed, these physical and chemical parameters significantly regulate cellular uptake, membrane adsorption, membrane transport, as well as the fate of the NPs in the cell and their delivery to the specific organelle. The morphology of the prepared TSPO-QD@SiO_2 NPs, investigated by TEM analysis (Figure 1C), reveals that NPs are of nearly 29 nm, quite monodisperse ($\sigma_{\%}$ = 7%), and with a core-shell structure, characterized by either multiple or single QD cores in a silica shell. The TEM investigation highlights that no significant aggregation or modification in QD@SiO_2 nanostructure geometry has occurred upon functionalization (See Electronic Supplementary Information Figure S 1B) and QD@SiO_2 NPs preserves their original size and size distribution.

Hydrodynamic diameter, colloidal stability and surface charge density of the luminescent QD@SiO_2 NPs, by means of DLS analysis and ζ-potential measurements, have been investigated at each functionalization steps, starting from the QD@SiO_2 NPs, to NH_2-QD@SiO_2 NPs, and finally to TSPO-QD@SiO_2 NPs (Figure 3).

DLS analysis clearly points out, for each step, a monomodal size distribution, thus suggesting that no NP aggregation occurs in aqueous medium and an increase of the average diameter passing from the "*as synthesized*" QD@SiO_2 NPs to the TSPO-QD@SiO_2 NPs, as expected due to the TSPO conjugation (Figure 3A). In particular, average diameter of 37 (PDI 0.175 ± 0.020), 39 (PDI 0.188 ± 0.017) and 50 nm (PDI 0.190 ± 0.025) has been recorded for the nanostructures, respectively. The size measured for TSPO-QD@SiO_2 NPs with the TEM (~29 nm) differs from the DLS measurements. The reason is ascribable to the simple consideration that TEM observation is able to detect only the inorganic domain of the hybrid conjugated nanostructure. Conversely, the higher hydrodynamic diameter value (50 nm) resulting from the DLS investigation, accounts for, beside to the inorganic component, the presence of the TSPO ligand, functionalizing the NP surface, the hydration shell, and also the excess counterions.

Finally, ζ-potential measurements have elucidated the effect on surface charge of luminescent NPs at each step of the functionalization process. Upon grafting of amine groups, the negatively charged QD@SiO_2 NPs (-32.0 ± 2.0 mV, Figure 3B red line) become positive (14.6 ± 0.3 mV, Figure 3B blue line), in agreement with the literature reported values.[30] Further conjugation with the TSPO ligand results in an average ζ-potential value of 11.7 ± 0.7 mV (Figure 3B violet line). The slightly less positive value of TSPO-QD@SiO_2 NPs with respect to that of the amino functionalized sample can be ascribed to the decrease of the free amino groups present at the surface of TSPO-QD@SiO_2 NPs, due to their partial neutralization by the formation of a covalent bond with the carboxylic group of the targeting moiety. This evidence further confirms the success of the conjugation reaction. Furthermore, the positive ζ-potential value observed for NH_2-QD@SiO_2 and TSPO-QD@SiO_2 NPs suggests that the nanostructures are protonated and bear a positive charge at physiological pH. This feature is expected to promote first NP adhesion on the negatively charged cell membranes by electrostatic attractions, and then NP transport into the cytosol by adsorptive endocytosis.[1,2] Moreover, previous studies have widely demonstrated that positive charged nanostructures could also induce the endosomal escape through several different mechanisms, the most popular model of which is the osmolytic or so-called "*proton-sponge*" effect.[1,2]

In addition, the size of TSPO-QD@SiO_2 NPs, in the submicrometer regime, should ensure cellular uptake by the energy dependent endocytosis, which is usually limited to particles <100 nm or at most to a few 100 nm in diameter, as previously reported.[2] In this regard, Marrache et al.[2] have

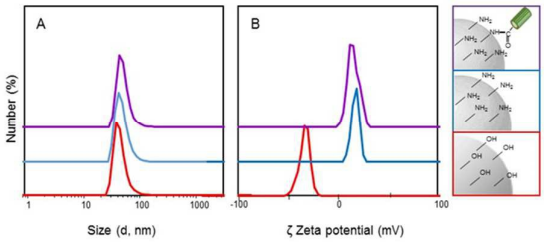

reported a systematic investigation on the effect of size and surface charge of TPP functionalized QDs in Hela cells. Indeed, the maximum cellular uptake has been observed for the smaller tested NPs (80-100 nm); keeping constant the NP hydrodynamic diameter, the cellular uptake has increased for the positive charged TPP functionalized QDs as the surface charge reached 1.3 mV and remained constant up to a surface charge of 22 mV, with increase mitochondrial uptake.[2]

Figure 3. Size distribution obtained by DLS (A) and ξ-potential measurements (B) of QD@SiO_2 NPs (red line), amino functionalized QD@SiO_2 NPs (blue line) and TSPO ligand-conjugated QD@SiO_2 NPs (violet line), along with a sketch of the silica surface.

In vitro cytotoxicity, intracellular fate and co-localization of NH_2-QD@SiO_2 and TSPO-QD@SiO_2 NPs in C6 rat glioma cells. The C6 rat glioma cells have been selected as an appropriate model to carry out cytotoxicity experiments, intracellular fate

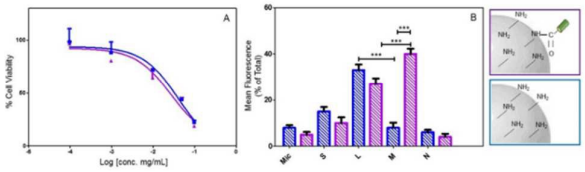

and co-localization studies, since they overexpress the mitochondrial receptor TSPO, thus resulting particularly suitable for the purpose of this work. In order to evaluate a suitable and non-toxic concentration of functionalized QD@SiO_2 NPs for further labelling experiments, the viability of C6 cells, incubated for long-term exposure (72 h) with NH_2-QD@SiO_2 NPs, before and after conjugation with the TSPO ligand, has been determined.

Figure 4. (A) Concentration-cell viability profiles for C6 rat glioma cells after 72 h of incubation with amino functionalized QD@SiO_2 NPs, (blue curve) and TSPO ligand-conjugated QD@SiO_2 NPs (violet curve). Each point represents a mean value of three independent experiments. (B) Subcellular fractionation of C6 cells after incubation with amino functionalized QD@SiO_2 NPs (blue bars) and TSPO ligand conjugated QD@SiO_2 NPs (violet bars). Key: microsomal (*Mic*), soluble (*S*), lysosomal (*L*), mitochondrial (*M*) and nuclear (*N*) fractions. Statistical values $p < 0.001$ (***) have been estimated using two-way ANOVA and Bonferroni post hoc test. Data represents mean ± SD, $n = 3$.

Figure 4A reports the profile of cell viability obtained by using the conventional MTT assay, varying the NP concentration in the range from 0.0001 to 0.1 mg/mL. The NH_2-QD@SiO_2 NPs and the TSPO-QD@SiO_2 NPs have affected the cell viability in a concentration-dependent way, giving the estimated IC_{50} values of nearly 0.040 ± 0.003 and 0.030 ± 0.002 mg/mL, respectively. Hence, the NH_2-QD@SiO_2 and the TSPO-QD@SiO_2 NPs have shown similar concentration-dependent toxicity. Therefore, for the further cellular labeling experiments the concentration of 0.010 mg/mL for both samples has been adopted, corresponding to a QD concentration of about 0.0045 µg/mL and 0.0033 µg/mL for NH_2-QD@SiO_2 and TSPO-QD@SiO_2 NPs, respectively.

In vitro cytotoxicity, intracellular fate and co-localization of NH_2-QD@SiO_2 and TSPO-QD@SiO_2 NPs in C6 rat glioma cells.

The C6 rat glioma cells have been selected as an appropriate model to carry out cytotoxicity experiments, intracellular fate and co-localization studies, since they overexpress the mitochondrial receptor TSPO, thus resulting particularly suitable for the purpose of this work. In order to evaluate a suitable and non-toxic concentration of functionalized QD@SiO_2 NPs for further labeling experiments, the viability of C6 cells, incubated for long-term exposure (72 h) with NH_2-QD@SiO_2 NPs, before and after conjugation with the TSPO ligand, has been determined.

Investigation of the intracellular fate and co-localization experiments of the TSPO-QD@SiO_2 NPs have been performed *in vitro,* in order to explore the ability of the synthesized nanostructure to enter the cells and target mitochondria. Quantitative and qualitative evaluation of the subcellular targeting of the synthesized TSPO-QD@SiO_2 NPs has been obtained by using two complementary techniques: namely subcellular fractionation and confocal laser scanning microscopy. In particular, for the first technique, C6 glioma cells have been exposed to each of the two types of NP samples (0.010 mg/mL) for 12 h and then fractioned into nuclear (*N*), mitochondrial (*M*), lysosomal (*L*), microsomal (*Mic*) and soluble (*S*) fractions by means of differential centrifugation.[27]

The characteristic PL of the QDs has been used to probe and quantify the amount of NPs bound to the cell membrane, and subsequently internalized into the cytoplasm or translocated to mitochondria.

Figure 4B reports the comparison of the mean PL (excitation set at 400 nm and emission wavelength at 570 nm) monitored for lysosomal (*L*), nuclear (*N*), microsomal (*Mic*), soluble (*S*) and mitochondria (*M*) fractions after exposition of C6 cells to amino functionalized or TSPO-QD@SiO_2 NPs. When the C6 cells have been treated with TSPO-QD@SiO_2 NPs, the mean fluorescence value obtained from the recovered mitochondrial fraction has been of about 40%. Significant PL intensity has been also detected in lysosomal fraction (27%), while less intense mean PL values have been recovered from nuclear (4%), microsomal (5%) and soluble (10%) fractions. Conversely, amino functionalized and not targeted luminescent NPs have provided a different intracellular distribution of the PL signals. Indeed, the mean PL value detected in the mitochondrial fraction (8%) was significantly lower than that observed for TSPO-QD@SiO_2 NPs. In this case, the higher PL intensity value has been recorded in the lysosomal fraction (33%), although a not negligible PL signal has been detected in the soluble fraction (15%). Finally, the mean PL value in the microsomal and nuclear fractions corresponds to 5 and 6 %, respectively (Figure 4B). The results obtained by subcellular fractionation study have clearly proven the occurrence of the cellular uptake of both targeted and not targeted grafted amine NPs, which seem to be able to cross and penetrate the extracellular membrane by endocytosis pathway. [36-38] Indeed, it is well documented that NP with ≤ 50 nm size and >10 mV surface charge can undergo to an enhanced cellular internalization through a nonspecific process, namely adsorptive endocytosis. Therefore, it is reasonably to assume that, in the investigated case, the positive charges at the surface of cationic grafted amine NPs (with ≤ 50 nm size and >10 mV surface charge) can promote ionic interactions with the anionic membrane components (such as membrane glycoproteins, proteoglycans) and initiate their rapid uptake, mainly *via* predominate clathrin-mediated endocytosis, trafficking the NPs to acidic endosomal/lysosomal compartments.[12] Indeed, PL intensity values recorded for the lysosomal fraction of both targeted and not targeted grafted amine NPs seem to suggest that their cellular uptake occurs by means of the mechanism previously described, indicating that NPs are rooted in the endocytic vesicles during the clathrin-mediated endocytosis, and, when unable to escape from them, are finally trapped in lysosomes. Otherwise, the NP localization in subcellular compartments different from lysosomes have also definitely established the ability of a significant fraction of NPs to disrupt the endosomal organelles reaching the cytosolic space in living cells. The endosomal escape observed for the both targeted and not targeted NPs could be mainly attributed to the osmolytic or so-called "*proton-sponge*" effect, which has been widely reported in literature as the most popular model of mechanism suitable to justify the escape ability of cationic NPs from endo-lysosomal compartments[39] Such an effect relies on proton absorption by buffering capacity of the excess uncharged amines on NPs into the endosomal compartment, inhibiting local acidification and forcing transmembrane ATPase proton pumps to transport additional protons and counter anions into the endosome to achieve the required pH as the vesicle matures towards late endo-lysosome. This differential in ionic strength induces osmotic swelling and eventual rupture of the endosomal membrane, ultimately causing the release of the

luminescent NPs into the cytosol and making them possibly accessible for mitochondrial targeting.[40]

In addition, according to a different mechanism, the membrane rupture of organelles, such as endosomes and lysosomes, could also take place thanks to the electrostatic attraction between the positive charged NP surface and negatively charged membrane organelle.[41] Interestingly , the PL intensity value (40%) recovered in the mitochondrial fraction, after cell incubation with TSPO-QD@SiO_2 NPs, univocally proves the high selectivity of the TSPO-QD@SiO_2 NPs to perform the mitochondrial targeting when their endosomal escape and subsequently release in cytosolic environment occur. Conversely, the not targeted NH_2-QD@SiO_2 NPs localize mainly in lysosomal and soluble fraction, as expected (Figure 4B). These results point out that only the TSPO-QD@SiO_2 NPs are selectively delivered and hence detected in the mitochondria, confirming the efficiency of the molecular recognition of TSPO ligand toward the specific mitochondrial membrane receptor, even upon its anchoring at the silica surface. Furthermore, remarkably, the subcellular localization study demonstrated that the mean PL intensity value recovered in the mitochondrial fraction has been of 40% for TSPO ligand QD@SiO_2NPs (versus 8% for not targeted NPs), while for the previously reported nanostructures based on G(4)-PAMAM–FITC dendrimers, the mean PL intensity value recovered in the mitochondrial fraction has been of 39% for the TSPO targeted versus 21% for the not targeted G(4)-PAMAM–FITC dendrimers.[27]

Such a comparison clearly points out a higher localization specificity in the mitochondrial subcellular compartment of the colloidal luminescent NPs with respect to the G(4)-PAMAM–FITC dendrimers, thus proving also their superior selectivity to achieve the mitochondrial targeting.

Further evidence of cellular uptake and mitochondria targeting has been achieved by cellular co-localization studies. The images in Figure 5 report C6 glioma cells incubated with fluorescent NH_2-QD@SiO_2 NPs (Figure 5 upper Panel) or TSPO-QD@SiO_2 NPs (Figure 5 bottom Panel) and investigated by confocal laser scanning microscopy in live cells, in order to avoid the artefactual results that may arise following fixation of cells prior to imaging.[27] The confocal laser scanning microscopy investigation confirms the high quality and robustness of the QD@SiO_2 NPs as, even at very low explored

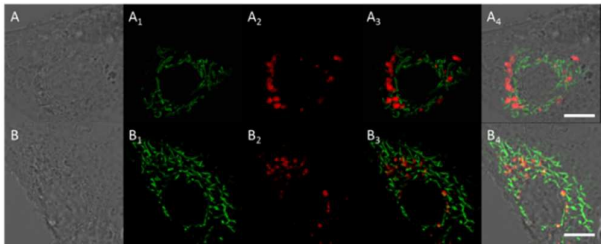

concentration of QDs, in the nanogram range. A high PL sensitivity has been achieved without any photobleaching occurring under continuous light exposure not only during image acquisition, but also for repeated set of experiments and much longer periods.

For the cellular co-localization studies, the red PL characteristic of the QD core provides the QD@SiO_2 NP localization while the MitoTracker green, used as specific mitochondria marker, allows location of the mitochondria. Superposition of PL images results in multiple-channel fluorescence image that merges the contribution of both probes and represents an efficient tool to evaluate co-localization.

Figura 5. Representative single confocal slices of live C6 cells imaged incubated with amino functionalized QD@SiO_2 NPs (A, A_1, A_2, A_3, A_4) and TSPO ligand-conjugated QD@SiO_2 NPs (B, B_1, B_2, B_3, B_4). Bright field (A, B), green (A_1, B_1), red (A_2, B_2) and detection channel and overlay (A_3, A_4, B_3, B_4). Scale bar = 10 µm.

Images in bright field (Figure 5 Panel A, B), green (Figure 5 Panel A_1, B_1) and red (Figure 5 Panel A_2, B_2) detection channels are reported in Figure 5 along with the overlay images (Figure 5 Panel A_3, B_3 and Panel A_4, B_4). Interestingly, the confocal microscopy of cells incubated with the TSPO targeted NPs reveals that most of the red areas (Figure 5 Panel B_2) converges to yellow in the overlay picture (Figure 5 Panel B_3), as a results of QD PL overlapping the green PL of the specific mitochondria marker (Figure 5 Panel B_1). This optical evidence and the concomitant lack of overlap of the red QD PL and the green mitochondria marker in the overlay panel of the NH_2-QD@SiO_2 NPs sample (Figure 5 Panel A_3) can effectively support the subcellular portioning results. These evidences, together, confirm the selective delivery of the TSPO ligand targeted QD@SiO_2 NPs to the mitochondria. In addition, a co-localization experiment has been performed, under the same conditions, in the presence of lysosomal marker, LysoTracker green. TSPO targeted NPs and NH_2-QD@SiO_2 NPs, have been

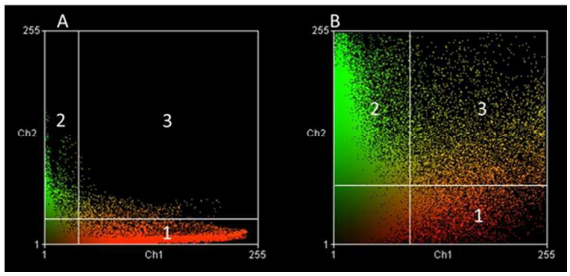

found both to co-localize at lysosomal level, in agreement with the proposed mechanism of cellular uptake by endocytosis. (See Electronic Supplementary Information Figure S 4)

The results of fluorescence co-localization studies are represented graphically in scatterplots, where the intensity of one color is plotted against the intensity of the second color for each pixel (Figure 6). Pixels of both channels having identical positions in the image can be regarded as a pair. In the scatter region 3 the co-localizing pixels are presented. The co-localizing pixels measured for NH_2-QD@SiO_2 NPs and TSPO-QD@SiO_2 NPs are 7% and 58% of the total, respectively, highlighting that the results obtained using subcellular fractionation and confocal microscopy are in good agreement.

Figure 6. Representative co-localization analysis in a double tagged C6 glioma cell. All pixels forming A3 and B3 images, referring to C6 cells treated with amino functionalized

$QD@SiO_2$ NPs and with TSPO ligand-conjugated $QD@SiO_2$ NPs, respectively, in Figure 5, are displayed on the A and B scatter diagram. The two channels of the images are compared. Pixel of both channels having identical position in the image can be regarded as a pair. Accordingly, each pixel pair has two intensities, one for each channel. The intensities of the two channels are reported along the axes of the scatter graphs. In the scatter region 3 the pixels that are co-localized are displayed.

In addition, the corresponding Manders' overlap coefficients, calculated for non-targeted and targeted nanosystems, as a mean on three different independent images, are 0.09 and 0.49. The higher Manders coefficient value measured for the TSPO-$QD@SiO_2$ NPs confirms the co-localization of the green and red detection channel, which are the green mitochondrial marker and the red QD PL, respectively. This outcome confirm undoubtedly that only TSPO-$QD@SiO_2$ NPs have been selectively delivered to the mitochondria, while almost negligible specific localization at mitochondria of the NH_2-$QD@SiO_2$ NPs has been achieved.

Conclusions.

The development of hybrid multifunctional nanomaterials based on luminescent QDs as bioimaging agent able to recognize the translocator protein has been reported. Namely a TSPO targeted imaging nanosystem has been effectively synthesized by using NH_2-$QD@SiO_2$ NP as a platform to be covalently linked to the high-affinity conjugable TSPO ligand, presenting a derivatizable carboxylic end group. The $QD@SiO_2$ NPs have demonstrated a suitable scaffold able to conveniently anchor the TSPO ligand, which in turn retained its ability to recognize the mitochondrial protein. The synthetized TSPO targeted luminescent QD-based nanomaterial shows the characteristic fluorescence of QDs and an absorbance spectrum that combines QD and TSPO ligand features. The nanosystem has positively charged surface, size in the submicrometer range with a hydrodynamic diameter of about 49 nm and a narrow size distribution. The ability of TSPO-$QD@SiO_2$ imaging agent to be internalized into C6 glioma cells and target a specific mitochondrial protein has been assessed by means of subcellular fractionation and confocal microscopy. The overall results univocally demonstrates the ability of the TSPO-$QD@SiO_2$ NP to specifically target the mitochondria, while almost negligible specific localization at mitochondria of the NH_2-$QD@SiO_2$ NPs has been detected.

Furthermore, the TSPO targeted nanosystems are highly luminescent and robust single object nanoarchitectures, combining an extraordinary resistance to photobleaching under continuous light exposure during confocal microscopy images acquisition, with a strong selectivity of the ligand towards TSPO. The resulting luminescent multifunctional nanomaterial possesses a unique selectivity as mitochondrial imaging agent and consequently a significant potential impact to future applications in biomedical field, both in diagnostics and therapeutics.

Materials and Methods.

Materials. The CdSe@ZnS QDs synthesis and surface processing were achieved through the following reagents: Cadmium oxide (99.5% powder, CdO), Trioctylphosphine oxide (99%, TOPO), *t*-Butylphosphonic acid (98%, tBuPOH), Hexadecylamine (technical grade 90%, HDA, Fluka), Tributylphosphine (97%, TBP), Selenium (99.99% powder, Se), Sulfur (99.9999% powder, S), Trioctylphosphine (90%, TOP), Diethylzinc solution (1 M in heptanes, Et_2Zn), Hexamethyldisilathiane (HMST). The silica shell growth was carried out by Tetraethyl orthosilicate (98% d = 0.934 g/mL, TEOS), Aqueous ammonia (d = 0.900 g/mL, NH_4OH), 5 polyoxyethylene nonylphenylether (Igepal CO-520, Mn=441), and surface functionalization with (3-Aminopropyl)triethoxysilane (97%, APS). For Ninhydrin test, Ninhydrin and 2,6-lutidine (98%, Alfa Aesar) were used. For the conjugation reaction (Benzotriazol-1-yloxy)tris(dimethylamino)phosphonium hexafluorophosphate (97%, BOP), *N*,*N*-diisopropylethylamine (99.5% DIPEA) were used. All chemicals, purchased from Sigma Aldrich if not specified otherwise, were used without purification. The TSPO ligand 2-(6,8-dichloro-2-(4-hydroxyphenyl)imidazo[1,2-a]pyridin-3-yl)-*N*,*N*-dipropylacetamide (MW= 477 g/mol) was prepared according to synthetic procedures reported elsewhere.[27] C6 rat glioma cells, from Interlab Cell Line Collection (ICLC, Genova, Italy), were grown in DMEM high glucose medium supplemented with 10% heat-inactivated fetal bovine serum (FBS), 100 U/mL penicillin, 100 µg/mL streptomycin and 2 mM L-glutamine (Lonza, Italy) in a 5% CO_2 humidified atmosphere at 37 °C.

Disposable culture flasks and Petri dishes were from Corning, Glassworks (Corning, N.Y., USA). 3-(4,5-dimethylthiazolyl-2)-2,5-diphenyltetrazolium bromide (MTT) was purchased from Sigma-Aldrich (Milan, Italy).

Synthesis of $QD@SiO_2$ NPs and functionalization with TSPO ligand. A silica shell was grown onto the "*as synthesized*" CdSe@ZnS QDs (d = 4 nm and relative standard deviation $\sigma_{\%}$ = 20%, see paragraph 4.3 for more information and Figure S 1A), emitting at 567 nm (see Electronic Supplementary Information), by using a water-in-oil microemulsion approach.[31, 34, 42, 43] A cyclohexane solution of QDs ($1.5x10^{-6}$ M) was prepared and 350 µL of IGEPAL CO-520, 200 µL of NH_4OH and 30 µL of TEOS were sequentially injected. The solution was then kept under vigorous stirring and controlled temperature 28 °C for 18 h. Collection and purification of the $QD@SiO_2$ NPs (d = 26 nm, and percentage relative standard deviation $\sigma_{\%}$ = 15%, see paragraph 4.3 for more information and Figure S 1B) were carried out by centrifugation and the NPs were finally dispersed in 2 mL of ethanol. The sample was lyophilized and 2.4 mg/mL of $QD@SiO_2$ were collected (QD concentration 1.1 µg/mL with a concentration of 10^{13} NP/mL)

Surface functionalization of $QD@SiO_2$ NPs with amine groups is carried out by using APS: 80 µL of APS ($6.8x10^{-4}$ mol) were added to a diluted suspension of $QD@SiO_2$ NPs (400 µL of $QD@SiO_2$ NPs diluted to 2 mL ethanol) under basic pH condition (80 µL of ammonia solution) and the final suspension was stirred overnight at 28 °C.[34] The NH_2-$QD@SiO_2$ NPs were collected by centrifugation and purified from unreacted

reagents by repeated cycle of centrifugation/redispersion in ethanol and finally dispersed in 1.5 mL of ethanol (0.6 mg/mL NH_2-QD@SiO_2 NPs . Amine groups titration of the NP suspension was carried out by using a ninhydrin test.[33, 44, 45] The ninhydrin solution was prepared by dissolving 110 mg of ninhydrin in 16 mL of ethanol (0.68% w/v) and 4 mL of 2,6 lutidine. 950 µL of the ninhydrin solution was added to 50 µL of NH_2-QD@SiO_2 NPs, warmed up at 80 °C for 10 min. The suspension turns light blue due to the formation of the Ruhemann's Blue by-product, which accounts for the presence of amine groups, and has an UV-Vis absorbance spectrum centred with a band centered at 570 nm. From the absorbance intensity at the maximum absorbance wavelength (570 nm) of the by-product, after plotting the calibration curve (ε = 2020 ± 90 L mol^{-1} cm^{-1}), concentration of primary amine groups was calculated from the Lambert-Beer law of nearly 5.4 ± 0.1 mM (0.60 mg/mL of NH_2-QD@SiO_2 NPs collected from lyophilized sample, with a QD concentration of 0.28 µg/mL)

Conjugation reaction of the TSPO ligand to the NH_2-QD@SiO_2 NPs were carried out by mixing suitable amount of NH_2-QD@SiO_2 NPs (400 µL) and TSPO ligand in ethanol (1.5 mL) in the presence of BOP and DIPEA, cross coupling agents. The reagents were mixed keeping constant, at 5, the NH_2 groups: TSPO ligand molar ratio (2.2 µmol of NH_2 groups and 0.44 µmol of TSPO ligand) and using the crosslinking agents according to the TSPO content as follows: DIPEA:TSPO ligand 3:1 and BOP:TSPO ligand 1.2:1 molar ratio, respectively. The suspension was stirred at room temperature for 48 hours and the TSPO-QD@SiO_2 NPs were collected by centrifugation at 7800 g for 10 min (Beckman J2-21), purified by three cycles of redispersion in ethanol/centrifugation and dispersed in 1 mL of ethanol for further spectroscopic characterization (0.30 mg/mL of TSPO-QD@SiO_2 NPs with a QD concentration of 0.1 µg/mL). The TSPO content in TSPO-QD@SiO_2 NP sample was determined by first creating of a calibration curve (Electronic Supplementary Information Figure S 3A). In particular, UV-Vis absorbance spectra were recorded as a function of TSPO concentration in ethanol and the calibration curve was obtained by plotting the absorbance intensity at 254 nm *versus* the TSPO concentration. The linear fitting of the scatter plot allows to determine the absorbance extinction coefficient, which is $\varepsilon_{254\ nm}$ = 35945 ± 710 L mol^{-1} cm^{-1}. Finally, once the extinction coefficient was known, the content of TSPO conjugated onto QD@SiO_2 NPs was calculated by using Lambert-Beer law, measuring the absorbance intensity at 254 nm for the TSPO-QD@SiO_2 NP sample. In order to remove the contribution of the QDs and of other scattering phenomena to the absorbance intensity at 254 nm, the NH_2-QD@SiO_2 suspension was used as baseline.

Transmission Electron Microscopy (TEM). Transmission electron microscopy (TEM) analysis has been performed by using a JEOL 100, operating at 100 kV. TEM images have been acquired by a Quemesa Olympus CCD 11 Mp Camera. The samples were prepared by dipping the 300 mesh amorphous carbon coated Cu grid in a nanoparticle suspension in ethanol, and letting the solvent to evaporate. Size statistical analysis (average NP size and relative standard deviation ($\sigma_{\%}$) for each NP sample) was performed by means of a freeware Image J analysis program.

Spectroscopic characterization. A Cary Varian 5000 UV-visible-NIR spectrophotometer was used to record the UV-Vis absorbance spectra.

The photoluminescence spectra were recorded using a spectrofluorimeter Fluorolog 3 (HORIBA Jobin-Yvon) equipped with double chromator reticles in excitation and emission. All optical measurements were carried out at room temperature. Relative PL quantum yield was measured by dispersing the samples in dimethylsulfoxide (DMSO) and using cumarine 153 in DMSO as standards (absolute QY in DMSO 75%) due to its spectroscopic properties (emission centered at 530 nm and excitation spectra in the range of 370-450 nm, thus suitably matching the emission spectrum range of QDs). The excitation wavelength used for the PL QY measurements was 395 nm.

Infrared spectra were recorded with a Perkin-Elmer Spectrum One Fourier transform infrared (FTIR) spectrometer equipped with a DTGS (deuterated triglycine sulphate) detector. The spectral resolution used for all experiments was 4 cm^{-1}. For attenuated total reflection (ATR) measurements, the internal reflection element (IRE) was a three-bounce, 4 mm diameter diamond microprism. The film samples were directly cast onto the internal reflection element by depositing the solution of interest (10 µL) on the upper face of the diamond crystal and allowing the solvent to evaporate completely.

Particle size, size distribution and surface charge. Hydrodynamic diameter (size), size distribution and colloidal stability of the NPs, before and after bioconjugation reaction with TSPO ligand, were detected using a Zetasizer Nano ZS, Malvern Instruments Ltd., Worcestershire, UK (DTS 5.00). In particular, size and size distribution were determined by means of dynamic light scattering (DLS) after dilution of NP aqueous solution (borate buffer, 50 mM, pH 8.5) in demineralized water. Hydrodynamic diameter is reported by number and size distribution is described in terms of polydispersity index (PDI). The ζ-potential measurements, *i.e.* the surface charges, were carried out by using a laser doppler velocimetry (LDV) after dilution of NP aqueous solution (borate buffer, 50 mM, pH 8.5) in KCl aqueous solution (1 mM). All reported data are presented as mean values ± standard deviation of three replicates.

Cell Culture and Cytotoxicity Assay. C6 rat glioma cells were maintained at 37 °C in an humidified incubator in the presence of 5% CO_2 in DMEM medium supplemented with 10% heat inactivated FBS, 2 mM L-glutamine, 100 U/mL penicillin and 100 µg/mL streptomycin.

The values of cytotoxicity (expressed as IC_{50}, namely the concentration of the tested substance to which the cell population is reduced by 50%) of the NH_2-QD@SiO_2 NPs and TSPO-QD@SiO_2 NPs were determined using the MTT assay (4,5-dimethylthiazol-2-yl)-2,5-diphenyl-tetrazolium bromide). The cells were seeded at a density of 5,000 cells/well into 96-well microtiter plates, and after incubation for one night, incubation of the samples, with concentrations ranging from 0.0001 to 0.1 mg/mL at 37 °C for 72 h was carried. Subsequently, addition of 10 µL of MTT 0.5% to the cells and

further incubation for further 3 h at 37 °C is performed. Finally, the cells were lysed by adding 100 µL of a solution of DMSO to each well. The absorbance at 570 nm was recorded by a Wallac Victor3, 1420 Multilabel Counter, Perkin-Elmer and the degree of cell viability calculated from the following equation using average absorbance value, as measured from three replicates,

$$\% \text{ Cell viability} = [A_{570\ nm,\ Sample}/A_{570nm,\ Control}] * 100$$

where $A_{570nm,Sample}$ is the mean absorbance at 570 nm recorded for each sample and $A_{570nm,Control}$ is the mean absorbance at 570 nm recorded from control cells (untreated cells).

Cellular fractionation. Cellular fractionation was obtained by means of differential centrifugation according to a literature reported.[26] In particular C6 glioma cells were fractioned into nuclear (*N*), mitochondrial (*M*), lysosomal (*L*), microsomal (*Mic*) and soluble (*S*) fraction. First of all, C6 cells were incubated for 12 h with NH_2-QD@SiO_2 NPs or, alternatively with TSPO-QD@SiO_2 NPs at concentration of 0.010 mg/mL. Afterwards extracellular content was washed away with cold PBS and then the pellet was washed once with homogenization buffer (250 mM sucrose, 10 mM HEPES, 1 mM EDTA pH 7.4) and a protease cocktail containing aprotinin (2 µg/mL), leupeptin (2 µg/mL), pepstatin A (1 mg/mL) and PMSF (1 mM). Then, differential centrifugation was carried out to collect the C6 cells cellular fraction. Each fraction was diluted with PBS and the fluorescence intensity at 570 nm (excitation wavelength at 400 nm), as arising from the QD luminescent core of the synthesized NPs, was measured on a microplate reader (Wallac Victor3, 1420 Multilabel Counter, Perkin-Elmer).

Confocal imaging on live cells. These experiments were carried out as previously reported.[26]

For live cell imaging, 10^5 C6 glioma Cells/well were seeded in glass bottom dishes (WillCo-Dish®) for 24 h and then incubated for 6 h with NH_2-QD@SiO_2 NPs or, alternately, TSPO-QD@SiO_2 NPs at a concentration of 0.010 mg/mL. The QD concentration was of about 0.0045 µg/mL and 0.0033 µg/mL for NH_2-QD@SiO_2 and TSPO-QD@SiO_2 NPs, respectively. The TSPO ligand concentration in the TSPO-QD@SiO_2 NP sample was $8x10^{-4}$ mg/mL. Subsequently, cells were treated with 100 nM MitoTracker Green FM, used as mitochondrial marker, or with 25 nM LysoTracker Green (Molecular Probes), used to label lysosomes, for 30 min at 37 °C and subsequently washed with phosphate buffer (PBS) lacking phenol at 25 °C. Cell images were acquired in the next 30 min using an inverted laser scanning confocal microscopy Leica TCS SP5-II (Leica Microsystems, Germany) equipped with ×63, 1.40 numerical aperture oil immersion lens. Laser beams with 405 nm and 488 nm excitation wavelengths were used for NPs (whose red emission come from the QD cores) and Mitotracker Green FM or LysoTracker Green (green emission) imaging, respectively and confocal microscopy scanning images of C6 rat glioma cells, 10-µm thick, were recorded in bright field and in red and green detection channel. Images were usually attained by using three line average and four frame average to increase signal to noise response. All data were subsequently processed with Leica LAS AF LITE (Leica microsystems, Germany) and ImageJ softwares.

Co-localization analysis. The intracellular localization of NH_2-QD@SiO_2 NPs or, alternately, TSPO-QD@SiO_2 NPs was investigated through co-localization analysis,[27] that evaluates the spatial and temporal overlapping in the distribution patterns of the two fluorescent probes, namely MitoTracker Green FM, used to label the mitochondria, and red emitting QDs, tagging the NPs. As far as digital imaging fluorescence emitted by the different fluorescent probes and occupying the same pixel in the image is intended as co-localization.

Following the generation of the scatterplot, it was possible to quantitatively evaluate the occurrence and the extent of co-localization. In this process, the scatterplot was used in combination with the fluorescence images in order to define the location of the co-localized fluorophores. Co-localization coefficients, which depend much on correct estimation of the image background and resolution, were calculated and for this purpose, preliminary image deconvolution was performed.

Different coefficients are reported to be used to estimate co-localization, here overlapping coefficient according to Manders was evaluated through.[46]

$$r = \frac{\sum_i S_{1i} \cdot S_{2i}}{\sqrt{\sum_i {S_{1i}}^2 \cdot \sum_i {S_{2i}}^2}}; 0 \le r \le 1$$

where S_{1i} and S_{2i} represent signal intensity of pixels in the channel 1 and in the channel 2. A major advantage of this coefficient is that it is not sensitive to differences in intensity among the components of an image caused by different labeling with fluorochromes, and so it is not sensitive to photo-bleaching or different settings of the amplifiers. Co-localization analysis was been performed by using software ImageJ.

Statistic. Statistical significance was assigned to $p < 0.001$ (***) and calculated using a one-way analysis of variance (ANOVA) followed by the Bonferroni post hoc tests (GraphPad Prism version 5 for Windows, GraphPad Software, San Diego, CA). Where indicated, standard error of the mean (SD) for data points was been calculated and the number of experiments indicated (*n*).

Acknowledgements

The University of Bari (Italy), the Italian Ministero dell'Università e della Ricerca [MIUR; FIRB RBFR122HFZ, PON R&C 2007–2013 MAAT-Molecular Nanotechnology for Health and Environment (Project number: PON02_00563_3316357), PRIN 2010–2011 NANO Molecular Technologies for Drug delivery (NANOMED)], NANOMAX-Integrable sensors for pathological biomarkers diagnosis (N-CHEM) and the Inter-University Consortium for Research on the Chemistry of Metal Ions in Biological Systems (C.I.R.C.M.S.B.) are gratefully acknowledged for the technical and financial support. The authors are grateful to Prof. Daniela Zanchet (Instituto de

Química, Campinas, Brazil) for the high resolution Transmission Electron Microscopy characterization.

Notes and references

1 R. K. Pathak, N. Kolishetti, S. Dhar, *Nanomed Nanobiotechnol.*, 2015, **7**, 315.
2 S. Marrache, S. Dahr, *PNAS* 2012, **109**, 16288.
3 L. Y. T. Chou, K. Ming, W. C. W. Chan, *Chem. Soc. Rev.* 2011, **40**, 233.
4 S. Fulda, L. Galluzzi, G. Kroemer, *Nat. Rev. Drug Discov.*, 2010, **9**, 447.
5 D. Peer, J. M. Karp, S. Hong, O. C. Farokhzad, R. Margalit, R. Langer, *Nat. Nanotechnol.*, 2007, **2**, 751.
6 L. M. Wang, Y. Liu, W. Li, X. M. Jiang, Y. L. Ji, X. C. Wu, L. G.; Xu, Y. Qiu, K. Zhao, T. T. Wei, Y. F.; Li, Y. L. Zhao, C. Y. Chen, *Nano Lett*., 2011, **11**, 772.
7 B. A. D. Neto, J. R. Correa, R. G. Silva, *RSC Adv.*, 2013, **3**, 5291.
8 C. W. T. Lung, Y. Hong, S. Chen, E. Zhao, J. W. Y.Lam, B. Z. Tang, *J. Am. Chem. Soc.*, 2013, **135**, 62.
9 V. Biju, T. Itoh, M. Ishikawa, *Chem. Soc. Rev.*, 2010, **39**, 3031.
10 K. D. Wegner, N.; Hildebrandt, *Chem. Soc. Rev.*, 2015, **44**, 4792.
11 A. Hoshino, K. Fujioka, T. Oku, S. Nakamura, M. Suga, Y. Yagamuchi, K. Suzuki, M. Yasuhara, K. Yamamoto, *Microbiol. Immunol.*, 2004, **48**, 985.
12 A. Chakraborty, N. R. Jana; *J. Phys. Chem. C*, 2015, **119**, 2888.
13 R. Rupprecht, V. Papadopoulos, G. Rammes, T.C. Baghai, J. Fan, N. Akula, G. Groyer, D. Adams, M. Schumacher, *Nature Rev.* 2010, **9**, 971.
14 C. Bento de Lima, E: K. Tamura, T. Montero-Melendez, J. Palermo-Neto, M. Perretti, R. P. Markus, S: H. Poliselli; F. Farsky, *Biochem. Bioph. Res. Co.*, 2012, **417**, 918.
15 L. Veenman, V. Papadopoulos, M. Gavish, *Curr Pharm Des.*, 2007, **13**, 2385.
16 J. Fan, M. B. Rone, V. Papadopoulos *J. Biol. Chem.* 2009, **284**, 30484.
17 A. Midzak, N. Denora, V. Laquintana, A. Cutrignelli, A. Lopedota, M. Franco, C. D.. Altomare, V. Papadopoulos, *Eur. J. Pharm. Sci.* 2015, **76**, 231.
18 N. Denora, V. Laquintana, A. Lopedota, A. Latrofa, J. M. Gallo, G Trapani, *Mol. Pharm.*, 2010, **7**, 2255.
19 V. Laquintana, N. Denora, A. Lopedota, H. Suzuki, M. Sawada, M. Serra, G. Biggio, A. Latrofa, G. Trapani, G. Liso, *Bioconjugate Chem.*, 2007, **18**, 1397.
20 V. Laquintana, N. Denora, T. Musacchio, M. Lasorsa, A. Latrofa, G. Trapani, *J. Control. Release*, 2009, **137**, 185.
21 M. Bai, D.J. Bornhop, *Curr. Med. Chem.* 2012, **19**, 4742.
22 K. Sekimata, K. Hatano, M. Ogawa, J. Abe, Y. Magata, G. Biggio, M. Serra, V. Laquintana, N. Denora, A. Latrofa, G. Trapani, G. Liso, *Nucl. Med. Bio.*, 2008, **35**, 327.
23 J. Salaklang, B. Steitz, A. Finka, C.P. O'Neil, M. Moniatte, A. J. van der Vlies, T. D. Giorgio, H. Hofmann, J. A. Hubbell, A. Petri-Fink, *Angew. Chem. Int. Ed.*, 2008, **47**, 7857.
24 O. S. Wolfbeis, *Chem. Soc. Rev.*, 2015, **44**, 4743.
25 N. Denora, V. Laquintana, A. Trapani, H. Suzuki, M. Sawada, G. Trapani, *Pharm. Res.*, 2011, **28**, 2820.
26 L. E. Samuelson, M. J. Dukes, C. R. Hunt, J. D. Casey, D. J. Bornhop, *Bioconjugate Chem*., 2009, **20**, 2082.
27 N. Denora, V. Laquintana, A. Lopalco, R. M. Iacobazzi, A. Lopedota, A. Cutrignelli, G. Iacobellis, C. Annese, M. Cascione, S. Leporatti, M. Franco, *J. Control. Release*, 2013, **172**, 1111.
28 A. Sperling, W. J. Parak, *Phyl. Trans. R. Soc. A* 2010, **368**, 1333.
29 A. Guerrero Marinez,, J. Perez-Juste, L. M. Liz-Marzan, *Adv. Mater.*, 2010, **22**, 1182.
30 M. Corricelli, N. Depalo, E. Di Carlo, E. Fanizza, V. Laquintana, N. Denora, A. Agostiano, M. Striccoli, M. L. Curri, *Nanoscale*, 2014, **6**, 7924.
31 E. Fanizza, N. Depalo, L. Clary, A. Agostiano, M. Striccoli, M. L. Curri, *Nanoscale* 2013, **5**, 3272.
32 C. Graf, Q. Gao, I. Schütz, C. N. Noufele, W. Ruan, U. Posselt, E. Korotianskiy, D. Nordmeyer, F. Rancan, S. Hadam, A. Vogt, J. Lademann, V. Haucke, E. Rühl, *Langmuir*, 2012, **28**, 7598.
33 N. Denora, V. Laquintana, M. G. Pisu, R. Dore, L. Murru, A. Latrofa, G. Trapani, E. Sanna, *J. Med. Chem.*, 2008, **51**, 6876.
34 E. Fanizza, C. Urso, V. Pinto, A. Cardone, R. Ragni, N. Depalo, M. L. Curri, A. Agostiano, G. M. Farinola, M. Striccoli, *J. Mater. Chem. C*, 2014, **2**, 5286.
35 M. R. Rasch, V. S. Konstantin, B. A. Korgel *Langmuir*, 2009, **25** 11777.
36 J. G. Huang, T. Leshuk, F. X. Gu, *Nano Today*, 2011, **6**, 478.
37 G. Xiao, L.-S. Gan, *Int. J. Cell Biology*, 2013, Article ID 703545.
38 S. J. Tan, N. R. Jana, S. J. Gao, P. K. Patra, J. Y. Ying, *Chem. Mater.* 2010, **22**, 2239.
39 L. Y. T. Chou, K. Ming, W.Chan, Chem. Soc. Rev. 2011, **40**, 233.
40 L. Y. T. Chou, K. Ming, W. C. W. Chan, *Chem. Soc. Rev.*, 2011, **40**, 233.
41 Z. Chu, Y. Huang, Q. Tao, Q. Li, *Nanoscale* 2011, **3**, 3291
42 R. Koole, M. M. van Schooneveld, J. Hilhorst, C. D. Donega, D. C.'t Hart, A. van Blaaderen, D. Vanmaekelbergh, A. Meijerink, *Chem. Mater.*, 2008, **20**, 2503.
43 P. Yang, N. Murase, M. Suzuki, C. Hosokawa, K. Kawasaki, T. Kato, T. Taguchi, *Chem. Comm.*, 2010, **46**, 4595.
44 E. Soto-Cantu, R. Cuento, J. Koch, P. S. Russo, *Langmuir* 2011, **28**, 556.
45 N. Depalo, L. Catucci, A. Mallardi, A. Corcelli, A. Agostiano, *Bioelectrochemistry*, 2004, **63**, 103.
46 E. M. M. Manders, F. J. Verbeek, J. A. Aten, *J. Microsc.*, 1993, **169**, 375.